Rapid Aero Modeling for Urban Air Mobility Aircraft in Computational Experiments

Patrick C. Murphy,[1] Pieter G. Buning,[2] and Benjamin M. Simmons[3]
NASA Langley Research Center, Hampton, VA, 23681

Rapid Aero Modeling (RAM) applied to computational testing, RAM-C, is an approach to efficiently and automatically obtain aerodynamic models during computational investigations. RAM-C is designed to estimate models appropriate for flight dynamics studies and simulations. The approach responds to a demand for experimental efficiency and model fidelity that has increased with growing aircraft complexity and aerodynamic nonlinearities associated with hybrid and electric vertical takeoff and landing (eVTOL) aircraft. In an Urban Air Mobility (UAM) transportation system, it is expected that aircraft will embrace many features from both airplanes and rotorcraft. These vehicles present many more factors than conventional aircraft which can lead to increased computational costs and missed key factor interactions when applying traditional testing and modeling methods. RAM-C provides feedback loops around computational codes to rapidly guide testing toward aerodynamic models meeting user-defined fidelity goals. It combines and extends concepts from design of experiment theory and aircraft system identification theory that allow the user the freedom to choose, in advance of the test, a specific level of fidelity in terms of prediction error. RAM-C only collects enough data required to meet the user-specified prediction error requirements thus saving computational time and resources. The overall achievable fidelity of the final model also depends on the accuracy of the test facility, or in this case, the computational modeling approach. Previous studies to support development of the RAM-T process were conducted in wind tunnel tests to assess potential metrics, algorithms, and procedures. This paper presents results from the next steps taken and tests conducted for the development of RAM-C technology and highlights some of the unique features of RAM applied eVTOL configurations in a computational study.

I. Nomenclature

B_i	=	regression coefficients
c_l	=	section lift coefficient
c_d	=	section drag coefficient
c_m	=	section pitching moment coefficient
e^*	=	normalized residual
e^*_{cv}	=	prediction error metric based on binomial analysis of residuals
NRMSE	=	normalized root-mean-square error
L, M, N	=	body-axis aerodynamic moments, ft-lbf
u, v, w	=	body-axis velocities, ft/s
X, Y, Z	=	body-axis aerodynamic forces, lbf
x_i	=	regressors
y	=	response variable in regression equation
α	=	angle-of-attack, deg
β	=	sideslip angle, deg
ε	=	error in regression model
σ	=	standard error

[1] Senior Research Engineer, Dynamic Systems and Control Branch, MS 308, Associate Fellow.
[2] Senior Research Scientist, Computational AeroSciences Branch, MS 128, Associate Fellow.
[3] Research Engineer, Flight Dynamics Branch, MS 308, Member.

II. Introduction

Aerodynamic modeling for flight dynamics studies plays an important role in any aircraft development program. This is especially true for many new complex vehicle designs proposed as part of an Urban Air Mobility (UAM) system that combine features of both conventional aircraft and rotorcraft. Under the Transformational Tools and Technologies and Revolutionary Vertical Lift Technologies Projects, NASA is recognizing the need for development of state-of-the-art computational and experimental tools and technologies required for development and prediction of future aircraft performance. Areas developing with increasing interest include autonomous systems, distributed electric propulsion, and electric vertical takeoff and landing (eVTOL) configurations. Market studies supported by NASA highlight the opportunities and difficulties for these areas both in terms of economics and technology [1-2].

The new design space offers significant opportunities, but it also creates vehicles with substantially more complex and nonlinear aerodynamic responses, as well as increased complex interactions among propulsion and aerodynamic control systems [3]. Resources required for modeling depend on the design stage considered where the levels of model fidelity typically increase as the design progresses. In early design stages, lower fidelity models may be sufficient for some aircraft configurations. However, eVTOL designs with the presence of rotors, propellers, tilting wings, control surfaces, and fuselage, result in a greater number of factors and interactions to consider, thus, significantly increasing design complexity that may reduce or defeat the utility of lower fidelity options. At any design stage, subject-matter experts (SME) will determine what level of fidelity is adequate for their problem.

The complexity issue drives demand for more resources to get suitable models for design and simulation. This can limit the ease of design changes while advancing through various design stages. Although advances in computer technology have facilitated more effective tools to tackle these issues, obtaining greater model fidelity still requires a significant investment of engineering time and resources both analytically and experimentally. Several research efforts to improve fidelity and efficiency have been made in ground-based testing [4-12], flight testing [13-18], and in computational methods [19-28]. The authors are also supporting current research by NASA in the UAM area [29-34].

One approach to improving the modeling process that reduces the various complexity issues, resource demands, and other adverse impacts described above is through development of a testing process called Rapid Aero Modeling (RAM). In a preliminary study of the RAM concept [33], consideration was given to determine potential metrics, algorithms, and procedures that would allow the RAM process to be implemented in an automated fashion. Experiments were performed on a conventional, off-the-shelf, radio-controlled model aircraft over a large flight envelope. These experiments followed the general RAM process; however, the process was guided manually without any automated decisions. The model, called the “Mini E-1,” is shown in Fig. 1. The experiment was designed to evaluate candidate procedures and metrics that might support the RAM process applied in a wind tunnel experiment, or also called a “RAM-T” application. Results from the preliminary RAM-T study indicated that the sequential automated testing process envisioned would be able to produce models below specified prediction errors.

Figure 1. Conventional aircraft (Mini-E1) in the NASA Langley 12-Foot Low-Speed Tunnel.

In this paper, a fully automated RAM process is demonstrated in computational experiments or “RAM-C” experiments. A fully automated RAM-T process is demonstrated in Ref. [34]. Applications of RAM-T and RAM-C to various configurations with combined airplane and rotorcraft features is an area of current research. In the first example of RAM-C, a basic rotorcraft airfoil (SSC-A09) [35], shown in Fig. 2, is tested over a large range of Mach

number and angle of attack to demonstrate RAM on a basic aerodynamic modeling problem. The example highlights two feedback loops in the RAM process. The first loop updates model order and the second loop updates test-region splitting after reaching model-order limits. For a second demonstration, aerodynamic models are developed for a hybrid rotorcraft-airplane vehicle proposed by NASA [36], called the Lift+Cruise (L+C). The L+C vehicle, shown in Fig. 3, is representative of complex vehicles being proposed for future UAM environments.

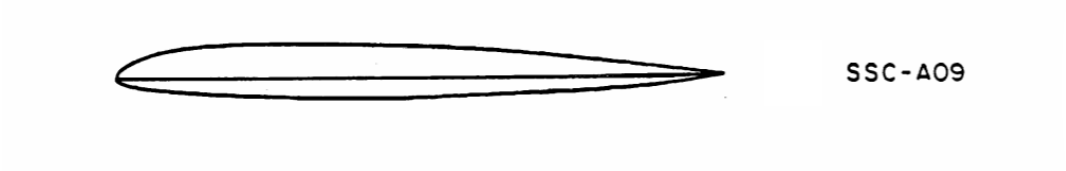

Figure 2. Rotorcraft airfoil (SSC-A09) profile, taken from NASA CR-166587 [35].

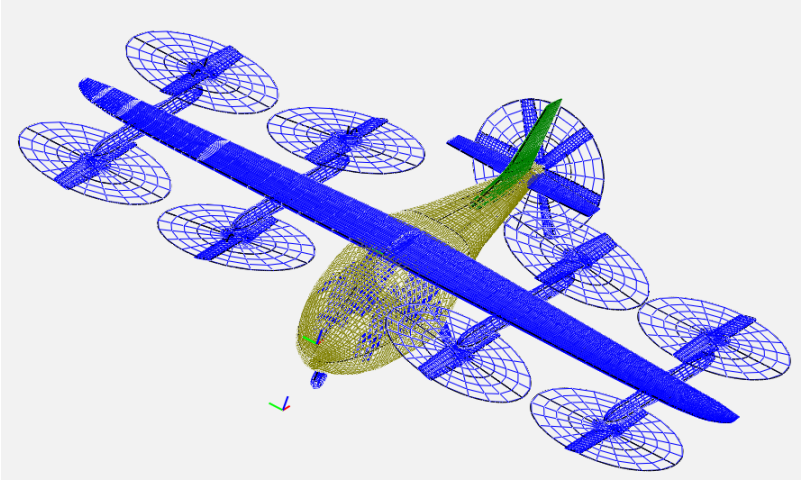

Figure 3. Lift+Cruise, a candidate research design for the UAM airspace.

III. The General RAM Process

One key objective for RAM is to develop aerodynamic models of general hybrid aircraft-rotorcraft configurations, such as eVTOL vehicles, intended for UAM applications that are suitable for nonlinear flight dynamics and controls simulations. RAM capitalizes on fundamentals from design of experiment (DOE) and aircraft system identification (SID) theory to form a unique automated modeling process. In addition to automating the modeling process while still allowing SME supervision, it offers an opportunity for significant savings in time and resources. A previous study [33] highlighted the initial development of the RAM process that provided statistically rigorous and efficient results by limiting the amount of data collected to that needed to achieve user-defined levels of fidelity. In this study, RAM is extended to an automated process and demonstrated for L+C, a hybrid aircraft-rotorcraft dual propulsion system eVTOL configuration. RAM is also used in application to a tandem tilt-wing, distributed electric propulsion configuration in Ref. [34]. Fidelity levels for RAM are defined in terms of model prediction errors. Of course, it is worth noting that the maximum achievable fidelity is also limited by the accuracy and measurement capabilities of the test apparatus and physical model under test, or in the case of RAM-C, the CFD methodology and fidelity of the geometric model.

An overview of the general RAM concept is presented in Fig. 4 as a simplified flow chart. On the left is the user-desired level of model fidelity and a sequence of pre-designed experiments in the form of sequential DOE blocks of test points appropriate for the vehicle under test. As the test facility processes each block to produce measurements for model identification, the resulting stepwise regression and Analysis of Variance (ANOVA) tables characterize the relative significance of model terms and other sources of variation. Effectively, the RAM process provides a control

loop around the vehicle under test that guides the test through a series of data blocks that are used to estimate models and evaluate their performance. The series of data blocks takes advantage of the sequential nature of designed experiments and only requests more data if it is needed for either estimating a higher-order model or for more detailed investigation in a region where model performance is inadequate. The test is completed when model validation tests are passed, indicating the requested level of fidelity is achieved. The test may also conclude when the limits of the test apparatus measurement capabilities are reached. The choice of identification methods, prediction error metrics, or how the test regions are split is not restricted by the general RAM process.

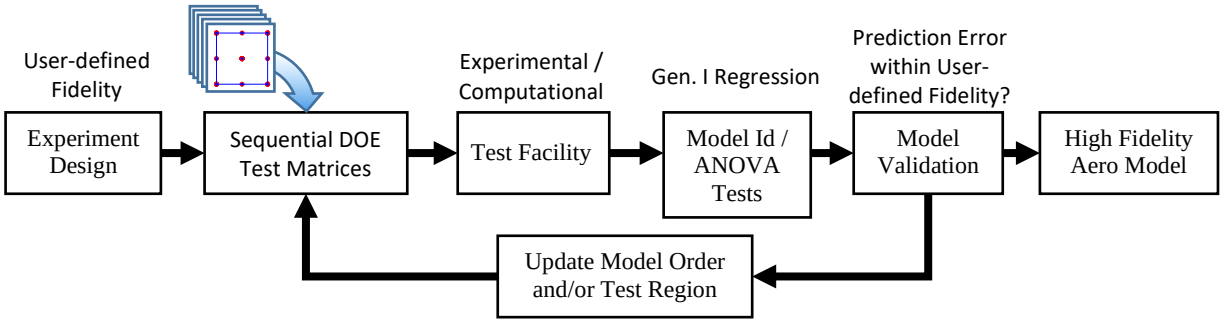

Figure 4. An overview of the RAM process.

Conventional experiments have been designed for use in wind tunnels and flight test for many years. Many of these practices are well established and have been demonstrated and corroborated through cross-comparisons with other tunnels, flight test, and computational methods. This traditional approach typically involves a controlled environment where one-factor-at-a-time (OFAT) methods are used to sweep over one of the states or controls of the vehicle under test while all other factors are held constant. Statisticians will disagree with the OFAT approach due to the possibility of unknown systematic errors being confounded with the data; however, practitioners go to great lengths to ensure that at least known systematic errors are minimized or eliminated. Conventional techniques have traditionally worked well for cases where the number of factors is limited to basic control surfaces and propulsion systems. However, for modern eVTOL designs, the number of factors can be anywhere from three to five times the number of traditional factors. This quickly overwhelms a conventional experiment design approach and limits the test from capturing possibly unexpected factor interactions as well as higher-order nonlinearities in any practical manner or time frame. This is especially true when time and resources are limited.

In the RAM approach the severity of these issues is reduced, if not eliminated, by taking advantage of well-established theory for model identification and experiment design. DOE theory is well documented and established in academia, industry, and government for a variety of applications. Credit for initial development of DOE is often given to Fisher [37]. DOE has since expanded and modernized from Fisher's agricultural applications to all fields of modern science and engineering.

A. RAM Flow Chart

The complete RAM algorithm is presented in Fig. 5 in flow chart form. To avoid confusion between flow-chart blocks and RAM data blocks, the flow chart blocks (FCB) are referred to using notation FCB (#). On the upper left are FCB (1-2) showing the general script for running RAM and a place for user inputs. User inputs define test features such as the factors, factor ranges, and user-desired level of model fidelity. FCB (3) provides a library of unique pre-designed test matrices in sets of five data blocks or test-matrix blocks, where each set is uniquely defined based on the number of factors involved for the test. These sets of blocks guide experiments through a sequential, optimized test points, where the sequence is designed to accommodate progressively more complicated models and minimize prediction errors. The sequential nature of the RAM process allows data collection to occur only when it is needed for either estimating a higher-order model or for a more detailed investigation in sub-regions where model performance is inadequate.

RiBjMk is used in the flow chart as an abbreviation to keep track of the i^{th}-region being modeled, jth-data block under test, and kth aircraft mode currently being evaluated. Aircraft modes are sometimes used to reflect significant configuration or mission changes such as speed regimes for vertical flight versus cruise flight. Details of the data blocks are given in Sec. III.B. In Fig. 5, FCB (4) converts the generic test matrices to reflect the initial factor ranges

specified by the user. This block also adjusts factor ranges when the regions under test are required to be split. FCB (5) converts the RAM information into a form appropriate for the test facility (TF). The test facility may be a wind-tunnel (WT), computational fluid dynamics (CFD), or simulated experiment (Sim), as shown in FCB (6). FCB (7) provides the conversion back from TF to RAM. FCB (8) denotes the user selected model identification procedure. For this study, stepwise regression is used and is discussed further in Sec. III.C. FCB (8) provides substantial output to the user (FCB (8a), (8b), (8c)) for monitoring progress. Outputs from the stepwise regression and Analysis of Variance (ANOVA) tables provide key statistics and characterize the relative significance of model terms. The next step in the RAM process is depicted in FCB (9). This block applies a prediction error (PE) test based on validation data not used for estimation. The PE test determines the progression of the RAM algorithm. If the PE test is passed, meaning the user-defined fidelity has been satisfied, then the final global model is estimated. If the PE test fails, then a decision is made to either use the next data block (test matrix) or split the region under test. The current version of RAM uses five data blocks that are used in sequence to reflect a progression from low-order models to high-order models. After each data block the RAM process uses the PE test to determine if more data is required, reflecting the need to estimate a higher-order model. In this study, polynomial models are limited up to third order. If the test in FCB (10) determines that all data blocks have not been used, then RAM proceeds to FCB (11) to obtain the next block. If the test in FCB (10) determines that all data blocks have been used, then RAM proceeds to FCB (12) to split the regions under study. Before proceeding back to FCB (4) to obtain the next test matrices, FCB (13) provides users an opportunity to check or adjust the RAM progression. The selection of optimal region partitioning is a current area of research and will add value to future RAM versions [38]. The final model represents a blending, FCB (14), over all the regions that may have been split during the RAM process. Individual polynomial models covering a subset of the factor space may not perfectly intersect with neighboring models at their boundaries, which creates a discontinuity between modeling regions. In order to blend neighboring models, the RAM software utilizes data from regions on both sides of the model intersection to create additional models spanning over the local intersections. The regions of overlap between local models are then smoothly combined using a polynomial weighting function. The results in FCB (15), indicate high fidelity (HiFi) models have been achieved.

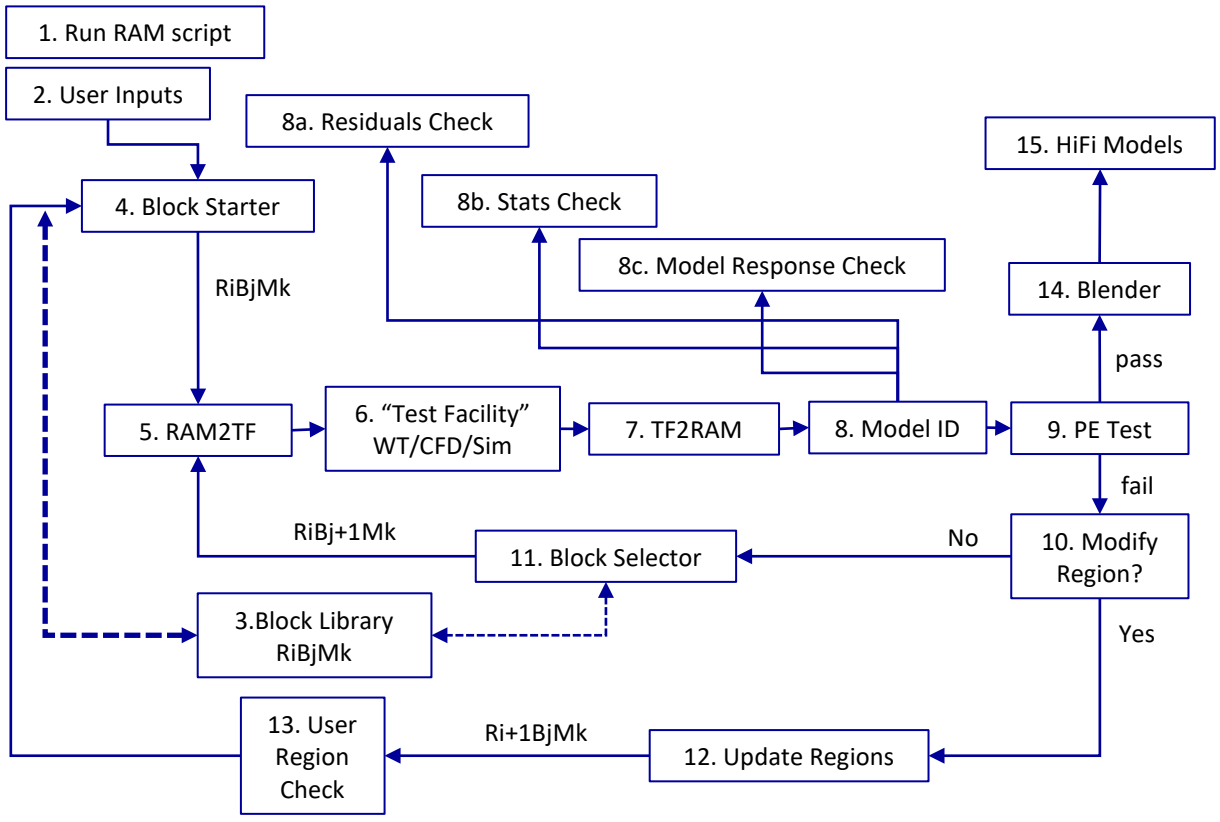

Figure 5. Detailed RAM process.

B. Experiment Design

In advance of performing an experiment, application of the well-developed DOE/response surface methodology (RSM) concepts provide guidance on setting up an efficient and statistically rigorous test plan as well as providing a much higher probability of obtaining an adequate model. For a RAM-based study, DOE/RSM theory is used to develop a specialized series of test matrices or data blocks that are applied in sequence. These data blocks are stored in the RAM Block Library and are constructed in coded space to improve numerical calculations and to allow more general application as factor ranges vary for each region tested. Ref. [31] expands on other considerations when using this approach. Coded form scales all the factors to lie in the range [-1, +1], as shown in Eq. (1).

$$\tilde{x} = \frac{x - (x_{\min} + x_{\max})/2}{(x_{\max} - x_{\min})/2} \tag{1}$$

For the current studies, RAM aerodynamic models use a polynomial model structure, although other model structures could be applied as well. In general, experiment design based on DOE is well documented in Ref. [39]. Five key principles of DOE support RAM and the sequential process to testing and modeling. The principles commonly used in DOE design are:

1. Orthogonal regressors – uncorrelated regressors to improve estimation calculations.
2. Replication – independent and repeated measurements to assess system noise and uncertainty.
3. Randomization – randomized input matrix to average out extraneous factors and unknown systematic errors.
4. Blocking – technique to improve precision and reduce variability due to known nuisance factors.
5. Sequential testing – a knowledge building process that allows each step to benefit from the previous one.

These principles provide important benefits to any designed experiment. For DOE tests in general, the concept of blocking serves to reduce miscellaneous nuisance bias errors. In RAM experiments, blocking and sequential testing serve an additional and primary purpose to perform sequential model identification that progresses from low-order models to higher-order models. Model identification allows only up to third-order polynomials and three-factor interactions. These higher-order terms typically appear in very limited numbers and, given the amount of data collected in a RAM process, the number of degrees of freedom for estimation is very high. As in any modeling process, final review of model terms is always required by subject-matter experts to ensure the estimated coefficients make sense for the application. Section IV.A discusses specialization of RAM block designs for experiments using computational or analytical methods as the test facility.

One classical DOE design is the factorial experiment [37]. A factorial design is one which varies all factors for all possible combinations. Using two levels for each factor represents a run-efficient method for developing a first order plus interaction model. A full-factorial design in two-factor space is shown below in Fig. 6 with the addition of a center point.

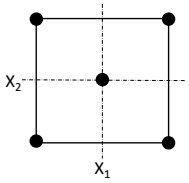

Figure 6. A full-factorial design in two-factor space.

Replicated centers allow testing for curvature that may suggest further augmentation is required to support quadratic model terms. This type of information allows the investigator to sequentially build models and only incorporate increasing amounts of data as required. The supported regression model is shown with up to two-factor interactions (2FI) by

$$y = B_0 + \sum_i B_i x_i + \sum \sum_{i \neq j} B_{ij} x_i x_j + \ldots + \varepsilon \qquad i = 1, 2, \ldots, k \tag{2}$$

The B_i, B_{ij}, are the fitted regression coefficients and the x_i are the factors (independent variables or regressors). A refinement (augmentation) to the factorial design is the central composite design (CCD) [40] which adds design points along the axes through the origin of the design space as shown by the square symbols of Fig. 7. This approach supports a full second order model given in Eq. (3).

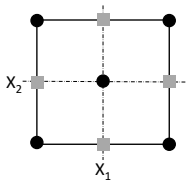

Figure 7. A face-centered central composite design in two-factor space.

$$y = B_0 + \sum_i B_i x_i + \sum_i B_{ii} x_i^2 + \sum \sum_{i \neq j} B_{ij} x_i x_j + \varepsilon \qquad i = 1, 2, ..., k \tag{3}$$

The location of the axial points defines this CCD as a face-centered design (FCD). The nested face-centered design allows the nesting of two FCD designs to support the addition of pure cubic terms to the empirical model. The two FCD's may be tuned by fractionating the factorial designs as presented by Landman [7]. The design in two-factor space is shown in Fig. 8 where the supported cubic model is given by Eq. (4).

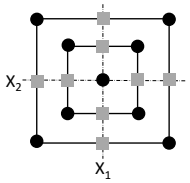

Figure 8. A nested face-centered design in two-factor space.

$$y = B_0 + \sum_i B_i x_i + \sum_i B_{ii} x_i^2 + \sum \sum_{i \neq j} B_{ij} x_i x_j + \sum_i B_{iii} x_i^3 + \varepsilon \qquad i = 1, 2, ..., k \tag{4}$$

DOE designs for RAM are developed as sequences of five blocks: (1) FCD, (2) nested FCD, (3) I-optimal designs that minimize prediction error for quadratic models, (4) I-optimal designs that minimize prediction error for up to cubic models, and (5) a final block to obtain validation data. Space filling designs have also been considered as alternate designs for blocks (4) and (5). The validation block can be applied separately at any point during the test but generally is taken at the start to allow validation tests throughout the experiment. The design choice of using five blocks is not a requirement but the authors have found it to be a reasonable choice for many cases. The series of blocks represent a progression of data collection that supports modeling polynomials from linear+2FI up to and including cubic+3FI. For cases with large numbers of factors, optimization to minimize prediction error can require machines with parallel processing capabilities. In cases where computational power is limited, the user may select a reduced-cubic model where an SME may assist in selecting key cubic or 3FI terms as appropriate.

Using polynomial model structures, limited to a maximum of cubic+3FI terms, can quickly lead to a requirement for dividing the global-model range into smaller regions. Polynomial models with higher-order terms than cubic can lead to parameter estimation problems and undesirable response and slope changes near the region end points. Fortunately, higher-order polynomials are unnecessary using the RAM splitting process. Splitting regions is performed on dominant factors with strong aerodynamic nonlinearities, such as angle of attack for conventional aircraft and forward velocity for rotorcraft. The split regions are blended in the final steps of RAM to provide continuous and smooth connections between split regions.

The transition region is the most challenging for modeling L+C and other complex eVTOL vehicles since all control surfaces and propulsors are used, the aerodynamics change rapidly with flight condition, and there are significant airframe-propulsion interaction effects. Figure 9 shows the splits in analysis of the transition region for

L+C. Color coding in Fig. 9 is used to indicate where models are successful (green) and where they fail (red). Splitting is discussed further in Sec. V with the final modeling results.

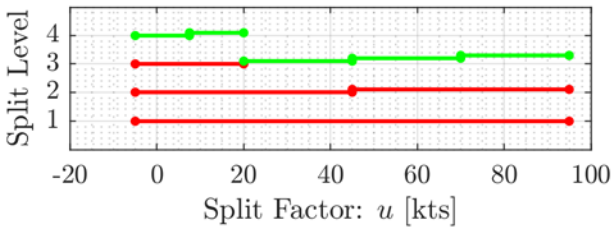

Figure 9. RAM-C speed regime splits for L+C study.

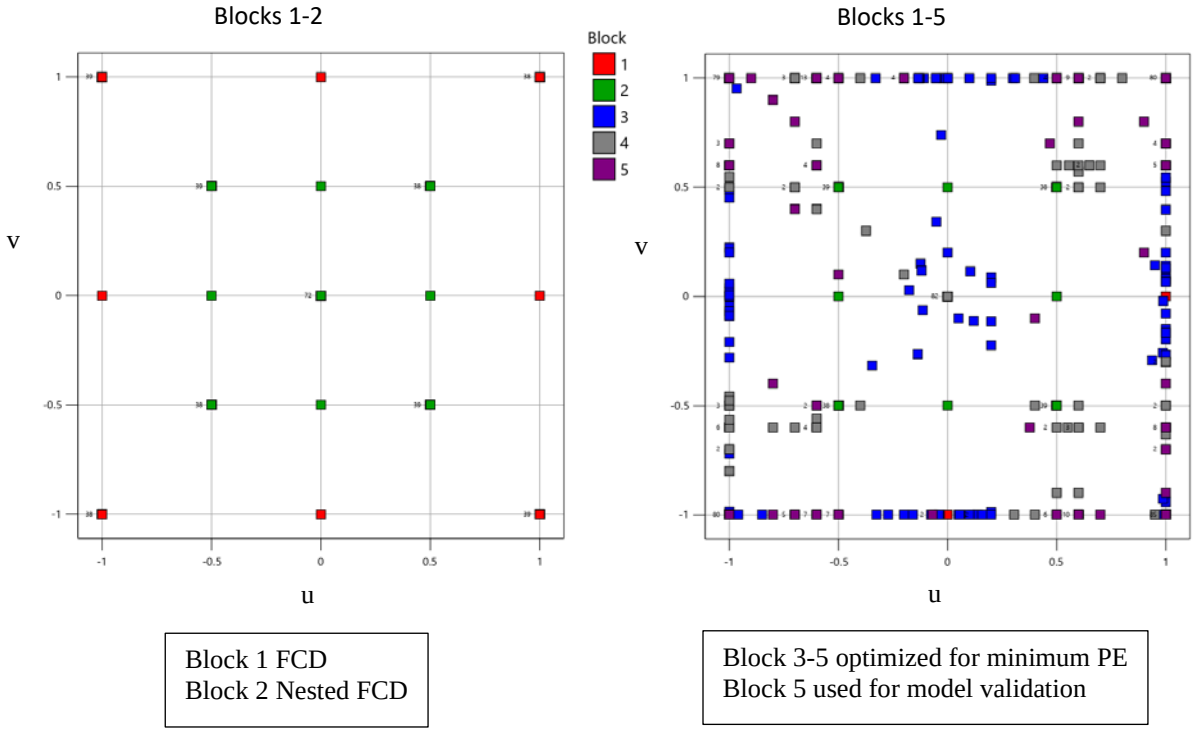

Figure 10. RAM data blocks for L+C, 17-factor study, in coded units.

Figures 9-10 and Tables 1-2 provide examples of the RAM experiment design and modeling process and provide a basis for the modeling results shown in Sec. V. An example five-block RAM design is shown in Fig. 10 for a 17-factor study of the L+C configuration. Blocks are shown in coded form. The two body-axis velocities (u, v) plotted in Fig. 10 produce a representative graphic for any two factors chosen from the set of 17 factors. The graphic on the left side shows separately the first two blocks to highlight the specific location of these test points. The graphic on the right side presents all five blocks to show the level of data density required for the RAM modeling process in this case. Blocks 3-5 are I-optimal designs that minimize prediction error. Table 1 provides a corresponding list of all 17 factors and their respective ranges.

Table 1. Factor Ranges for L+C Test in Transition Flight

#	Factor	Description	Range	Range	Units
	Label		Low	High	
1	*u*	body-axis *u*	-5	95	kts
2	*v*	body-axis *v*	-10	10	kts
3	*w*	body-axis *w*	-10	10	kts
4	LA	left aileron	-30	30	deg
5	RA	right aileron	-30	30	deg
6	LE	left elevator	-30	30	deg
7	RE	right elevator	-30	30	deg
8	RUD	rudder	-30	30	deg
9	n_1	Rotor 1	550	1550	rpm
10	n_2	Rotor 2	550	1550	rpm
11	n_3	Rotor 3	550	1550	rpm
12	n_4	Rotor 4	550	1550	rpm
13	n_5	Rotor 5	550	1550	rpm
14	n_6	Rotor 6	550	1550	rpm
15	n_7	Rotor 7	550	1550	rpm
16	n_8	Rotor 8	550	1550	rpm
17	n_9	Pusher-Prop	750	1750	rpm

Table 2. Maximum (worst case) values of sample design metrics (17 Factors) for L+C.

Block Type	Blocks	Pts.	Design Terms	VIF	FDS	% Power
	(inclusive)					2σ, s/n=2
Minimum Resolution V FCD	1	194	Quadratic	14.38	0.26	79.7
Nested FCD	1, 2	388	Quadratic	30.01	0.52	84.9
I-optimal	1, 2, 3	578	Quadratic	3.09	1.0	99.9
I-optimal	1, …, 4	783	Red. Cubic	13.99	1.0	99.9
Alternate (SFLH)	1, …, 4	783	Red. Cubic	11.20	1.0	99.9
Validation (I-opt)	1, …, 5	858	Red. Cubic	14.78	1.0	99.9
Alternate (SFLH)	1, …, 5	858	Red. Cubic	12.82	1.0	99.9

Table 2 shows some example design metrics used in building each DOE block. In this study each block was designed using either Design Expert [41] or JMP [42] software. As part of the experiment design work the investigator must define the confidence level required, signal/noise ratio for the test apparatus, and the minimum level of response detection required. However, in the execution phase, the investigator must also pre-define a level of acceptable prediction error for validation tests to confirm an adequate model and to prevent over-collecting data. As described previously, each block reflects the sequential collection of data that allows progressively more complex models to be estimated and the test only moves forward collecting more data if more complex models are required to meet PE requirements. Blocks 4 and 5 were developed using both I-optimal and as alternates space-filling Latin Hypercube (SFLH) designs. SFLH are popular experiment design choices for simulation studies [43]. Validation blocks are developed at the same time as the other blocks to ensure that the optimization selects validation points different from model estimation points.

The first design metric in Table 2 is the variance inflation factor (VIF) that reflects the degree of orthogonality for the regressors. Values of VIF are equal to one if regressors are perfectly orthogonal. Values over 10 reflect a degradation of orthogonality in certain regressors and may require further design evaluations. Fraction of Design Space (FDS) is a visual tool [41] for evaluating the standard error profile over the design space. This is the preferred metric when large numbers of factors are considered. The FDS number reflects the fraction of the design space within the expected variance parameters. For the design process, an assumption is made that standard deviation is 1 to allow relative predictive error to be computed. For this evaluation a very conservative assumption is made that the signal-to-noise ratio is only 2. The last metric indicates the experimental power (to avoid type 2 errors) for which values over 80% are acceptable. Maximum values of the design metrics shown in Table 2 were selected from a survey of all model

terms and selecting the worst-case term to show how each block design was progressing and improving the overall design as blocks of additional design points were added.

The first three of five RAM blocks in Table 2 present a sequence of designs that define the primary test sequence. The last two blocks are either I-optimal designs, based on minimizing the integrated prediction variance over the design space, or as an alternate design test, SFLH designs to evenly distribute test points over the entire space. For cases with large numbers of factors, as in this L+C example, the design metrics for the first three blocks were evaluated against a full quadratic model and the remaining blocks were evaluated assuming the presence of cubic terms without three-factor interactions. For cases with less numbers of factors, designs can be tested against models with cubic plus 3-factor interactions. The VIF values in block 2 show the cost of adding more data, in the form of a nested FCD, to capture potential cubic nonlinearities. The nested FCD is particularly useful in aerospace applications since it is designed to handle nonlinear responses and ensure the full ranges of factors are covered. This is particularly important for modeling aircraft surface deflections. I-optimal block 3 strategically adds new runs bringing all the design metrics to satisfactory levels. The first three blocks are often enough for modeling the aerodynamic coefficients, especially in the lower angle-of-attack region below stall, where models were expected to be mildly quadratic. Minor degradation to VIF is caused by adding block 4 but this is not an issue since the FDS metric, the preferred metric for response surface modeling, is still satisfactory. Block 4 provides additional modeling data to support modeling if model complexity demands the higher-order terms. Block 5 is also an optimal design and is used only for validation. Optimal blocks are useful for validation data since the optimizer avoids using existing design points.

C. Model Identification

The general process of guiding model identification in RAM, outlined in Sec. III.A, is applicable to both computational and physical test environments. A commonly used process for aircraft model identification was described briefly in the previous RAM study [33], and more generally in Ref. [44]. In this study, model identification methods used in RAM were adapted from the System Identification Programs for Aircraft (SIDPAC) software toolbox [44]. Results of model identification for a rotorcraft airfoil and the L+C configuration, in a fully automated RAM process, are provided in Sec. V. These results are obtained using a CFD test environment.

For this study, the primary method for model identification, specifically model structure determination and parameter estimation, is accomplished using stepwise regression. This is a well-known method and broadly used in many science and engineering applications. However, the RAM process does not restrict the user to a single method of model structure determination and parameter estimation. The identification process is improved for eVTOL configurations using models where the aerodynamic responses are defined in dimensional form and ranges for freestream velocity are defined in terms of body-axis velocities [31]. This approach allows more straightforward modeling of flight conditions representing slow transition, vertical, and hover flight, where freestream velocity can be zero or very small.

D. Validation

Three key objectives in the RAM modeling process are: (1) minimize standard error to get an adequate model fit, (2) minimize prediction error to get a useful model, and (3) only collect enough data to meet the precision, prediction, and validation requirements. These objectives reflect a balance among the precision demanded by the experimentalist, the capabilities or precision levels possible by the test apparatus, and the time and cost required to meet those demands. As demonstrated in Ref. [33], improvements made by decreasing fit error must be balanced against potentially increasing prediction error. The basic goal is to expand data collection only enough to meet the model complexity requirements. The validation step supports these objectives.

Validation, FCB (9), is a key step in the RAM process, used to test model performance. This step determines whether the estimated model is a good predictor of the system responses within user-defined bounds. The PE test provides a metric for this purpose. A practical method for assessing validation is to observe the residuals between measured and predicted responses. For well-designed experiments that result in adequate models, the residuals appear as white noise with magnitudes generally within the specified acceptable levels. Not every residual test point will meet the acceptable error boundary limit, however. As described in Ref. [45], success or failure of a given validation test-point residual to meet the requirement can be judged as a binomial (pass-fail) experiment. For complex vehicle tests where large numbers of data points are required, such as for the current L+C study, the RAM process uses 75 test points for validation. In that case, the critical binomial number is 66, based on models estimated at a 95% confidence level, and allowing only 1% inference error in the binomial test. This implies that the worst nine validation residuals define the level for an adequate model. If the residuals are normalized by the response variable maximum absolute value, defined as e^*, then the critical binomial number defines a benchmark or PE test metric, e^*_{cv}, that marks an

acceptable percentage of failed residual responses. For statistically small validation data sets, the preferred PE metric is the normalized root-mean square error (NRMSE) of the validation residuals. In either case, the PE test metric is simply a benchmark to assess how well the model predicts validation responses. The acceptable level of model fidelity is set by the investigator. Example applications of the two PE test metrics are discussed further in Sec. V.

Figure 11 shows an example case for the L+C axial-force, normal-force, pitching-moment normalized modeling and validation residuals after using all five blocks of data in a region with forward velocity between 20 kts and 45 kts. Validation points (block 5) are indicated by black triangles as a data point symbol. The residuals plotted against run number show no trends during the experiment and present an acceptable error process for regression, indicating no other variables or processes are confounded with the data. Included in the graphic are error bounds that show the prediction error (PE metric) achieved for this test.

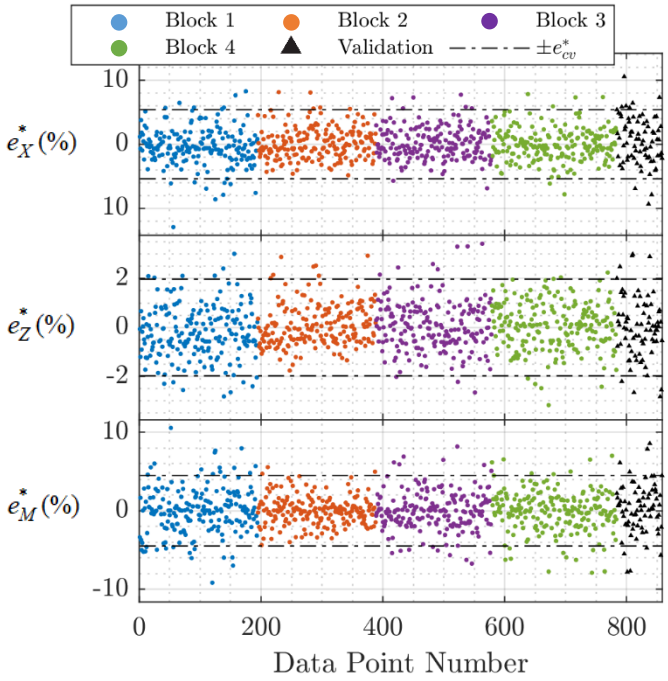

Figure 11. Example residuals for *X*, *Z*, and *M* models, L+C, 17-factor physical experiment.

IV. RAM-C Aerodynamic Modeling

Aerodynamic modeling reflects the objectives and intended use of the resulting mathematical models. The objective for RAM is to generate models that capture the important features of complex vehicles in a manner suitable for flight dynamics simulations. The same objective applies to RAM-C, except the goal is to obtain models from computational codes. For this study, the NASA OVERFLOW CFD code [25-27] is chosen to represent the "Test Facility" block in Fig. 5. Flight tests and wind tunnels offer alternate, excellent sources of aerodynamic information; however, these physical testing approaches require substantial investments of time and resources. Consequently, test efficiency is an important factor addressed by the RAM process. In early design stages, however, where conceptual designs need to be evaluated by several disciplines, the only practical source for aerodynamic information is from computational studies. Given the complexity of the vehicles under study, researchers are drawn to sophisticated computational simulations. However, for the flight dynamics and controls disciplines, detailed CFD models cannot produce results fast enough for real-time flight simulations. Aerodynamic models in the form of polynomial equations solve this issue, but these models must satisfy user-defined fidelity levels in order to have practical value.

A. RAM Applied to CFD

Application of RAM to computational experiments offers some benefits that cannot be realized in physical experiments. In simulated tests most factors are easy to change, unknown and known sources of variability are reduced or eliminated (limitations and assumptions made in the CFD code are set by the practitioner's choices), and random errors, in the form of measurement noise, are not present in either the inputs (regressors) or the outputs (responses).

Without measurement noise, the primary source of residual errors is due to modeling errors. This effectively eliminates requirements in designed experiments to include replication, randomization, and blocking of nuisance variables. However, designed experiments for RAM are developed with these design features remaining present. The benefit is to substantially reduces the size of the Block Library required for RAM with only a very small penalty in testing and analysis. Although replicated points do not provide new information, they represent a very small number of extra data points relative to the total number of points required for modeling a complex vehicle. And replicated points can be useful to monitor any simulation result changes, especially when using advanced CFD methods where changes in convergence criteria or unsteady aerodynamic regions can impact responses. Retaining randomization has no impact on analysis of simulated data and retaining blocking in RAM retains a primary goal of sequential modeling from lower-order to higher-order models.

Regression (ordinary least squares) analysis is a valid modeling technique when applied to either simulated or physical tests. Consider that six of the seven primary assumptions behind regression are still satisfied in a RAM-C test and analysis: (1) models are linear in the coefficients while regressors can be nonlinear, (2) residuals have a population mean of zero, (3) independent variables are uncorrelated with the residuals, (4) residuals are uncorrelated, (5) residuals present constant variance, and (6) independent variables are sufficiently uncorrelated (RAM designs optimize regressors to be as orthogonal as possible and minimize prediction errors). The last assumption (7) is that residuals are random and normally distributed. The assumption of normality is optional for application of ordinary least squares, but it is important to allow various statistical tests to be performed. For RAM-C normality is not required to obtain an unbiased and minimum variance regression model. However, the primary change when RAM is applied to simulated tests is that, although the models can provide accurate response predictions within the range of factors considered, no statements can be made about parameter confidence intervals, a mean response, or corresponding prediction intervals. In this case, the PE test metric simply becomes a device to assess relative model adequacy without any statement of confidence levels or prediction intervals. It is worth noting that for complex eVTOL vehicles, very large data samples are required which in turn can produce residuals that pass normality tests. Those cases are similar to physical experiments with extremely low noise levels.

B. CFD – Simulated Test Facility

The RAM-C process uses a computational method to produce aerodynamic forces and moments given the selected input factors. These factors include flight conditions and control inputs. A range of computational methods can be used, representing different levels of fidelity. Here, the NASA OVERFLOW CFD code [25-27] is used, which solves the compressible Reynolds-Averaged Navier-Stokes equations on a collection of overset, structured grids. The Chimera overset grid approach is particularly suited to multiple-body or moving body applications and has been used extensively for rotorcraft and UAM configurations [46-47].

The choice of computational method is a function of user expertise, available time and computational resources, as well as physical modeling fidelity required. In the case of eVTOL configurations, nonlinear interactions between vehicle components such as the wing, control surfaces, fuselage, and rotors can be important influences on the overall vehicle performance and on modeling requirements. Demanding flow conditions include hover, vertical flight, and transition, where rotor wash over the wing and tail has a significant aerodynamic effect (cf. Fig. 12). These complex conditions suggest the use of a CFD method; alternatives requiring less time and computational resources might include VSPAero [48], NDARC [49], or CAMRAD II [50].

For the Lift+Cruise configuration considered in this paper, a coarse computational grid of four million points was created. This included wing, fuselage, horizontal and vertical tails, and disks for the eight rotors and pusher propeller shown in Fig. 13. These latter components were modeled using a rotor disk methodology [51] rather than fully modeling rotating blades. This was done to reduce the grid size and to encourage steady-state flow solutions. The geometry was simplified by removing the support struts for the eight rotors, and the landing gear. To further simplify the gridding requirements, control surface deflections were modeled by deforming the surface grids, ignoring the gaps at the ends of each control surface. These approximations were justified on the basis that this was a proof-of-concept experiment. The goal was to produce an aerodynamic model that could be tested by the flight dynamics community and did not represent an actual flying vehicle. The current grid system is considered adequate to model basic interactions between rotor-induced flows and the vehicle structure, though grid refinement studies and unsteady flow simulations were not performed. These choices, and the tradeoffs with other computational methods will need to be revisited for an actual flight vehicle. With these approximations, each test point was calculated in two hours on one node (20 CPU cores) of the NASA Advanced Supercomputing (NAS) Pleiades system. Typical runs were made generating 50 test points simultaneously, limited by availability of resources on the system.

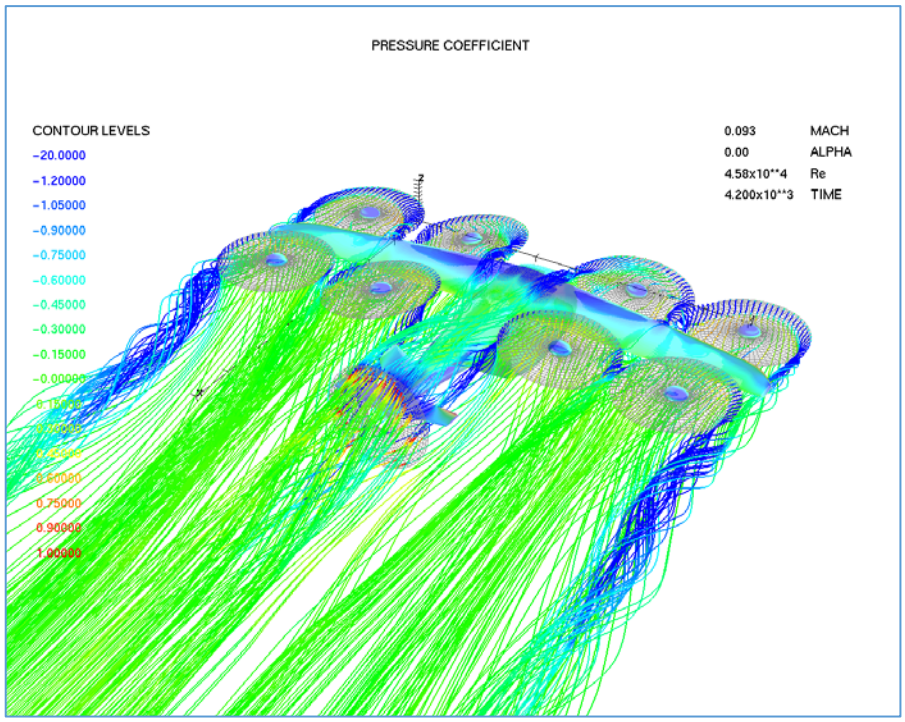

Figure 12. Lift + Cruise vehicle in horizontal flight with flow from rotors colored by pressure coefficient.

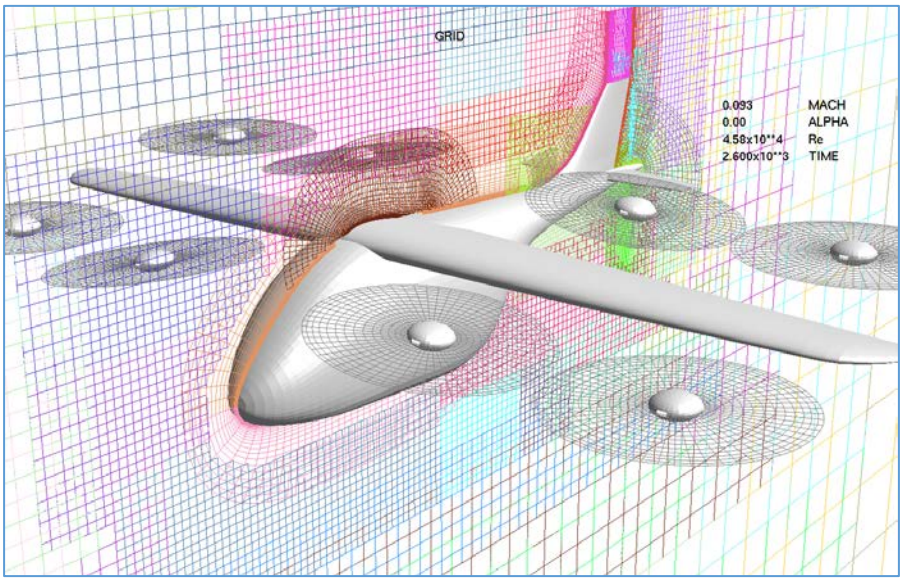

Figure 13. CFD overset grid system for Lift+Cruise vehicle.

V. RAM-C Modeling Examples

RAM-C is demonstrated by application to two modeling examples that show the wide range of modeling problems that can be handled by this method. The first case is an airfoil study to highlight how the RAM-C process can overcome common difficulties in modeling where significant nonlinearities are present in aerodynamic responses. The second case is an eVTOL configuration, L+C, demonstrating the utility of RAM-C for complex vehicles.

A. Airfoil Study

Application of RAM-C to a well-known rotor airfoil (SSC-A09) highlights the accuracy and efficiency of the modeling process for a simplified modeling problem with very few factors but with significant nonlinearities requiring the splitting process to achieve adequate models. Figure 14 presents an example SSC-A09 database. Variations in force and moment coefficients with Mach number and angle-of-attack illustrate the aerodynamic complexity possible even for cases with a limited number of factors.

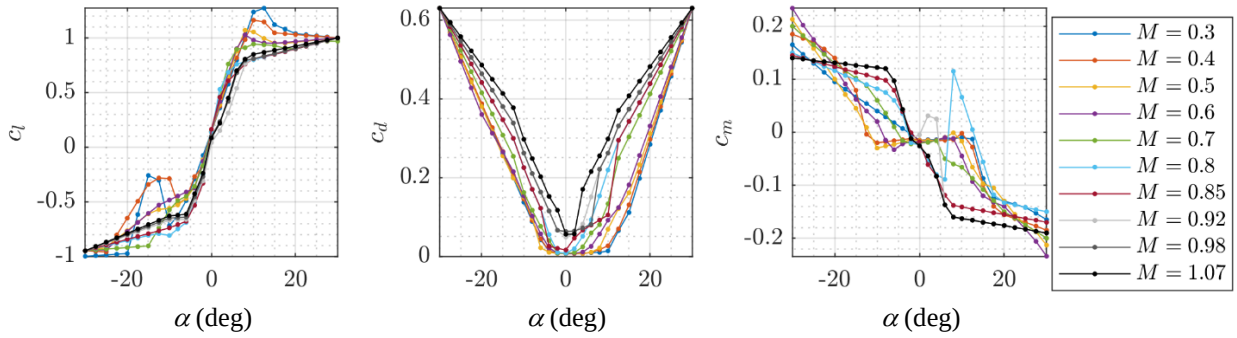

Figure 14. Aerodynamic coefficients of airfoil (SSC-A09) over range of alpha and Mach.

To demonstrate RAM-C applied to this airfoil in a computational study, the factors or explanatory variables and their ranges of interest are chosen as shown in Table 3. CFD, as described in Sec. IV.B is used as the "test facility" in this case. Although this case involves very few factors, the RAM process can still be applied. The adjustment in the RAM process occurs in FCB (4), the Block Library, where the appropriate sequence of blocks is chosen to correspond to the number of factors required.

Table 3. Factor Ranges for SSC-A09 Test

#	Factor Label	Description	Range Low	Range High	Units
1	α	Angle of attack	-30	30	deg
2	M	Mach	0.3	1.1	Non-dim

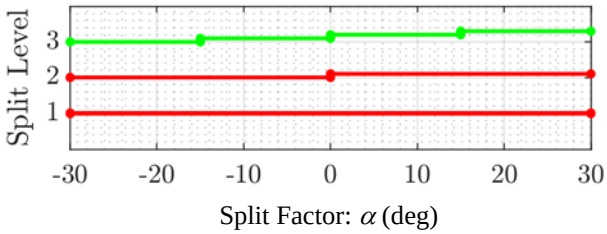

Figure 15. Splitting process for RAM airfoil (SSC-A09) study.

Figure 15 characterizes the region splitting that enables the RAM process to achieve more accurate models and ultimately achieve the desired final PE metric value. Level 1 (L1) is the full range of interest and represents Region 1 (R1). In this example, α is chosen as the key variable for splitting and the split sub-regions are made without any overlap. The choice of splitting on more than one variable and intelligent, automated region splitting (rather than splitting regions in half) will be incorporated as options in future versions of RAM. As shown in the figure, each new

level of splitting is labeled. After the first split of L1R1 into Level 2 (L2), two new sub-regions are produced, referred to as L2R2 and L2R3. For this example, satisfactory PE values (shown as green bars) were obtained using Level 3 (L3) splits. Figure 16 shows results of the modeling progress for each coefficient in terms of the PE metric. For computational studies with relatively few validation points (in this case only 15 validation points were computed in each sub-region), the PE metric is defined as the normalized root-mean-square error or NRMSE for validation data. Final models were considered satisfactory when the PE metric was either close to or below 5%. During the RAM modeling process for each sub-region, regression resulted in only cubic polynomials with 2-factor interactions required to satisfy the PE metric. Figure 17 shows the resulting model surfaces for each sub-region. To help assess the quality of model fit, a limited amount of the "measured" data is shown as black dots; the dots represent data along the mid-range values for each factor within each sub-region. The last step in the RAM process is to blend the final sub-region models for each coefficient into global polynomial models useful for flight dynamics simulations.

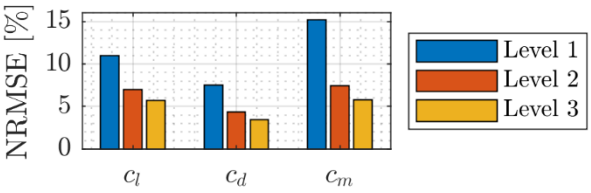

Figure 16. PE metric progress for each Level for airfoil (SSC-A09) study.

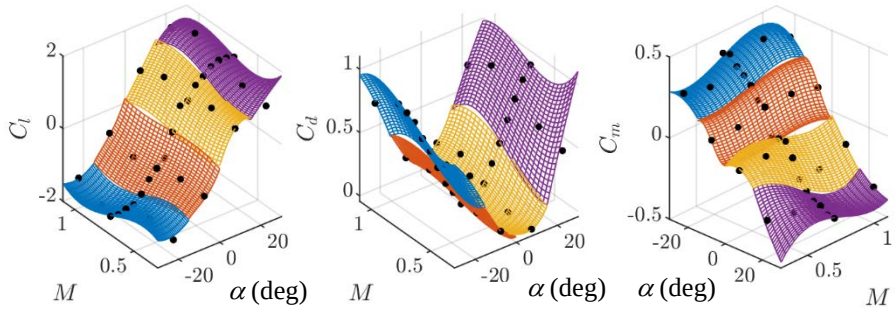

Figure 17. Aerodynamic coefficients for each sub-region for the SSC-A09 study.

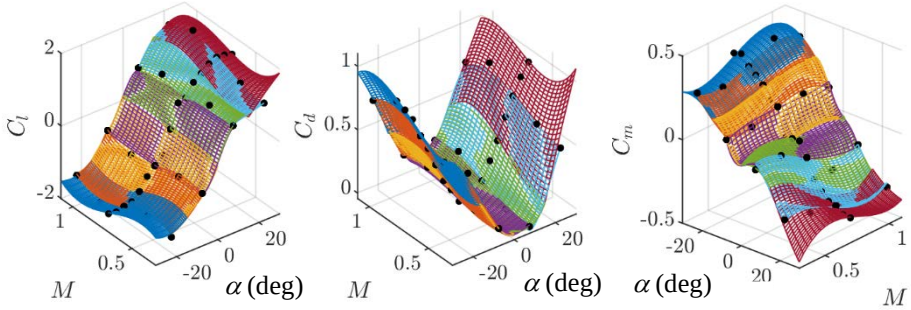

Figure 18. Aerodynamic coefficients for each sub-region after blending for SSC-A09 study.

Additional model fits used for blending each coefficient are shown in Fig. 18. Figure 19 shows the final global response surface model presented with color coding based on coefficient magnitude. A final check on residuals for the global models is given in Fig. 20, where the blue dots are residual data points covering all the final four sub-regions and the small black triangles are all the validation test points. The residuals generally are satisfactory; however, the C_d residuals reveal less desirable behavior when comparing the middle two regions (100 < data points < 300) with those outside that range. The outside regions include the highest angles of attack where fitting the data is more difficult and where unsteady behavior of the aerodynamics is more difficult to capture in CFD simulations.

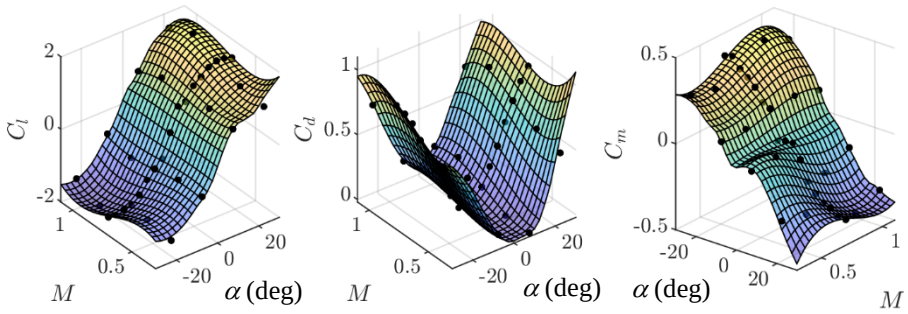

Figure 19. Final global aerodynamic coefficients for the SSC-A09 airfoil study.

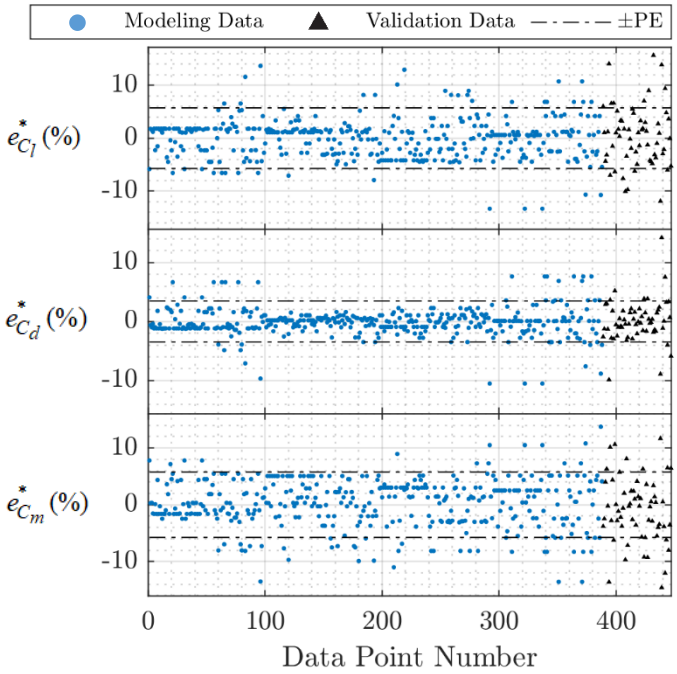

Figure 20. Residuals for SSC-A09 airfoil based on the final global model.

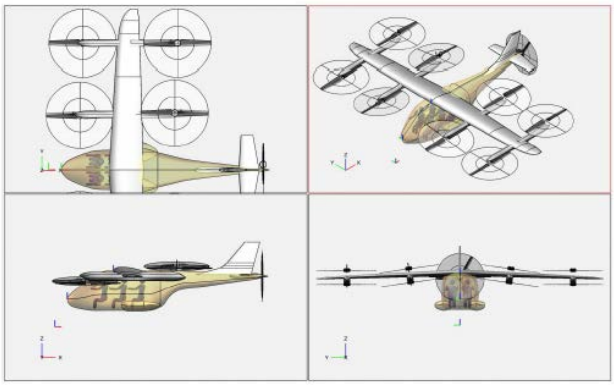

Figure 21. Lift+Cruise (L+C) vehicle geometry (Silva et al. [36]).

B. Lift+Cruise (L+C) Study

Application of a fully automated RAM-C process is demonstrated by application to a complex configuration called "Lift+Cruise" (L+C), shown in Fig. 3 and again in Fig. 21 with more geometry details [36]. The L+C configuration is provided to show application to a complex, rotor-dominated vehicle as well as an application using a high-fidelity computational code in a static test environment. An example simulation of L+C in a steady vertical-flight condition using the NASA OVERFLOW CFD code [25-27], is shown in Fig. 22. In this case, the vehicle is operating at 6000 ft with only the lift rotors running at mid-rpm. For demonstration of the RAM-C process, the transition modeling range is studied since it presents a challenging region to model with all propulsion and control surfaces operating.

Table 1 provides a list of the 17 factors considered for the L+C transition case. Modeling hybrid aircraft-rotorcraft vehicles is more practically accomplished using body-axis velocities (u, v, w) rather than velocity magnitude, angle-of-attack and sideslip angle (V, α, β). This is because at very low speeds the vehicle may fly at angles-of-attack and sideslip angles from -180 to +180 degrees, while at higher speeds the angle-of-attack and sideslip angles of interest are much more limited (cf. Fig. 23). For this type of vehicle (u, v, w) can be used to define fixed ranges for the independent variables while covering angle-of-attack and sideslip angle ranges of interest. For output variables, the use of dimensional forces and moments relieves the quandary of defining a consistent force and moment coefficient non-dimensionalization applicable to forward flight and hover, as well as multiple rotors operating at varying rpm. From a modeling perspective, it is important to note that both choices impact the form of the response surface and the ability of a polynomial-based model to fit that surface. In these simulations the eight rotors (n_1-n_8) and the pusher prop (n_9) are all modeled as fixed-pitch blades and with rpm control between representative values for idle and maximum rpm.

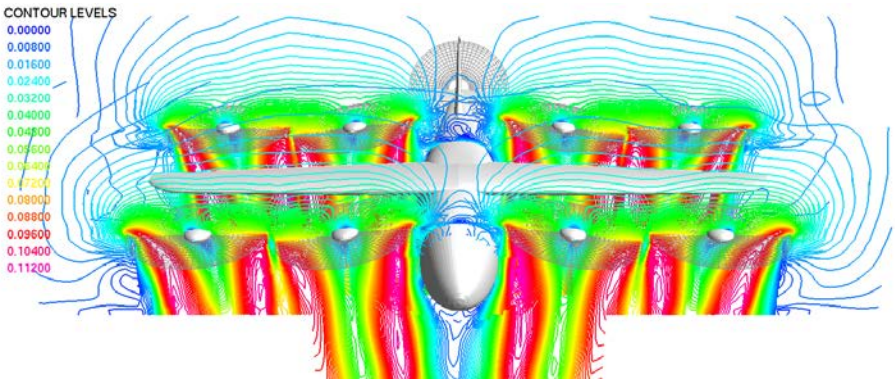

Figure 22. L+C velocity contours in simulated hover (based on OVERFLOW).

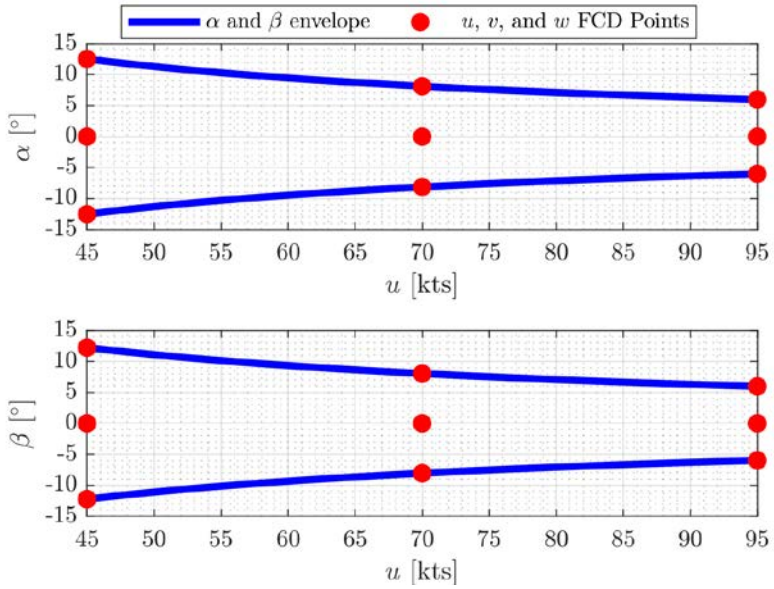

Figure 23. Angle of attack and sideslip envelopes for L+C transition study.

Figure 24 shows the region splits resulting from RAM-C applied to the L+C modeling study. Since a large range of forward velocity was initially addressed, four levels of splitting (producing five sub-regions) was required to obtain satisfactory PE metric values. In this study, splitting was performed on body-axis velocity, *u*, and sub-regions were developed with 0% overlap. As shown in the figure, at Level 4, only the lowest speed region required an additional split before the final models were deemed to satisfy fidelity requirements. In this case, polynomial models were estimated only up to quadratic terms plus 2-factor interactions.

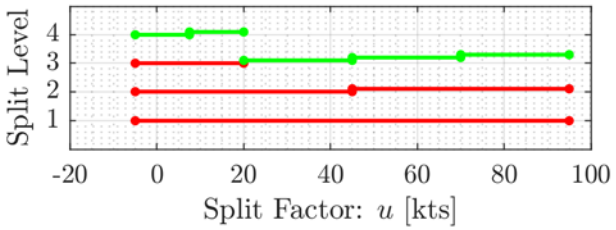

Figure 24. RAM splitting process for L+C transition study.

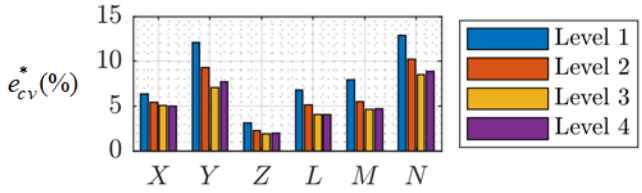

Figure 25. PE metric at each split level for L+C transition study.

Figure 25 shows the PE metric, in this case e^*_{cv}, achieved at each split level. These values generally improved moving from L1 down to L3 but adding L4 at very low speeds only helped axial force, X, and provided neutral benefit to Z, L, and M. For side force, Y, and yawing moment, N, PE values were slightly increased. In general, further improvement of the PE values can be accomplished with additional splitting or allowing higher-order polynomials. Engineering judgement can determine the practical limits on the number of splits that make sense. The last split for L4, added more validation points at very low speeds where the data presented much more variability making model prediction much harder. The increased variability in the computational data is shown in Fig. 29.

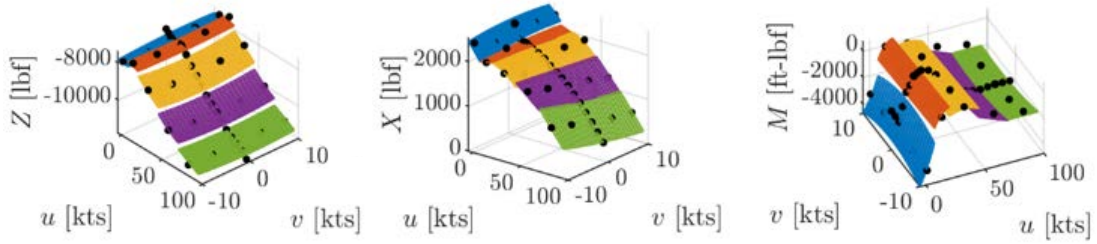

Figure 26a. Longitudinal response models for separate regions versus (*u, v*).

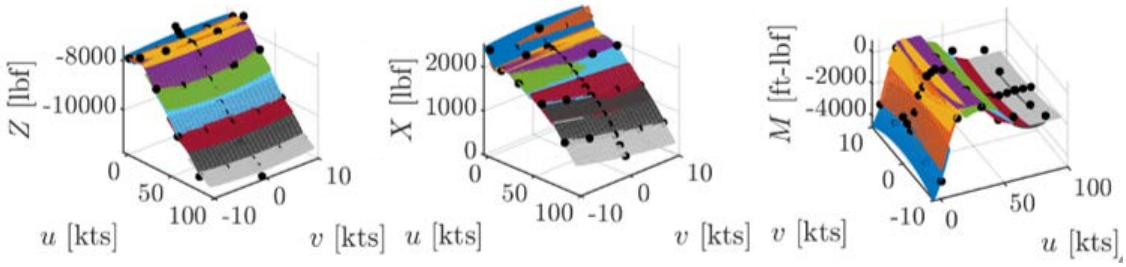

Figure 26b. Longitudinal response models for blended regions versus (*u, v*).

Figures 26a and 27a show example results for the longitudinal model surfaces for each sub-region as functions of (*u, v*) and (*u, w*), respectively. Figures 26b and 27b show the same model surfaces with the additional blending models also displayed. "Measured" data, selected along factor mid-range values, are shown as black dots.

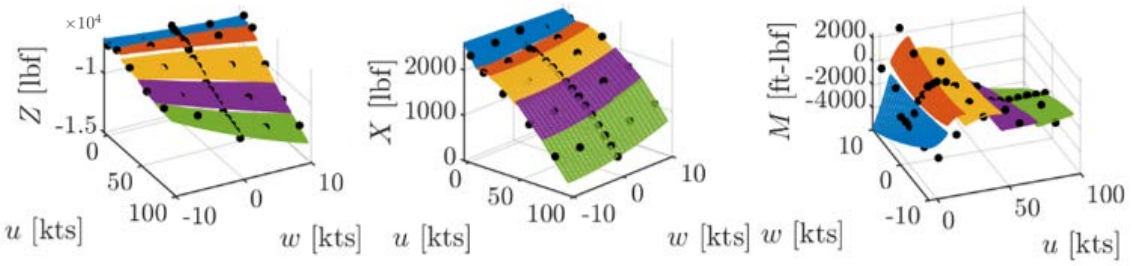

Figure 27a. Longitudinal response models for separate regions versus (*u, w*).

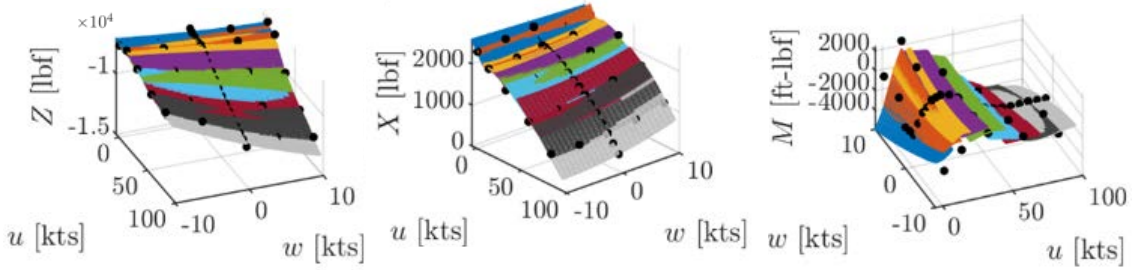

Figure 27b. Longitudinal response models for blended regions versus (*u, w*).

Model residuals normalized by the response global maximum absolute value are shown in Fig. 28. These residuals generally indicate satisfactory modeling results. Blue dots represent normalized residuals from model estimation data and black triangles are normalized residuals from validation data.

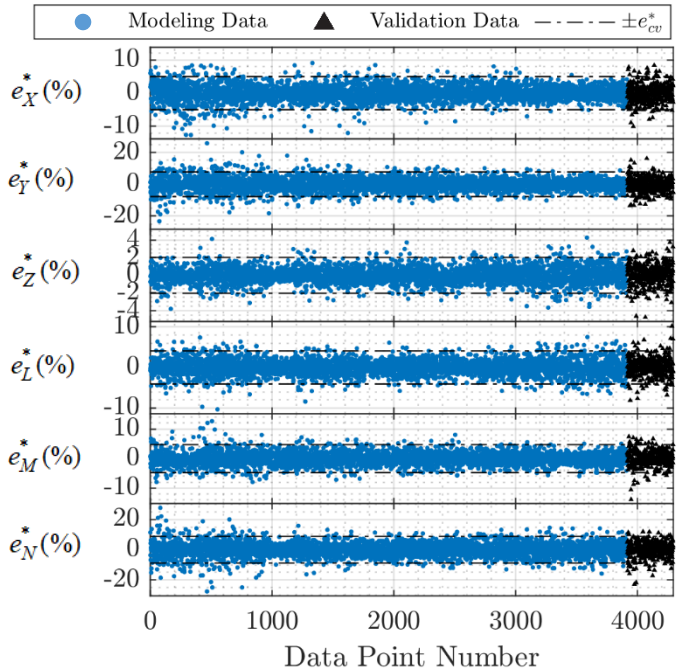

Figure 28. Residual plots for final coefficient models.

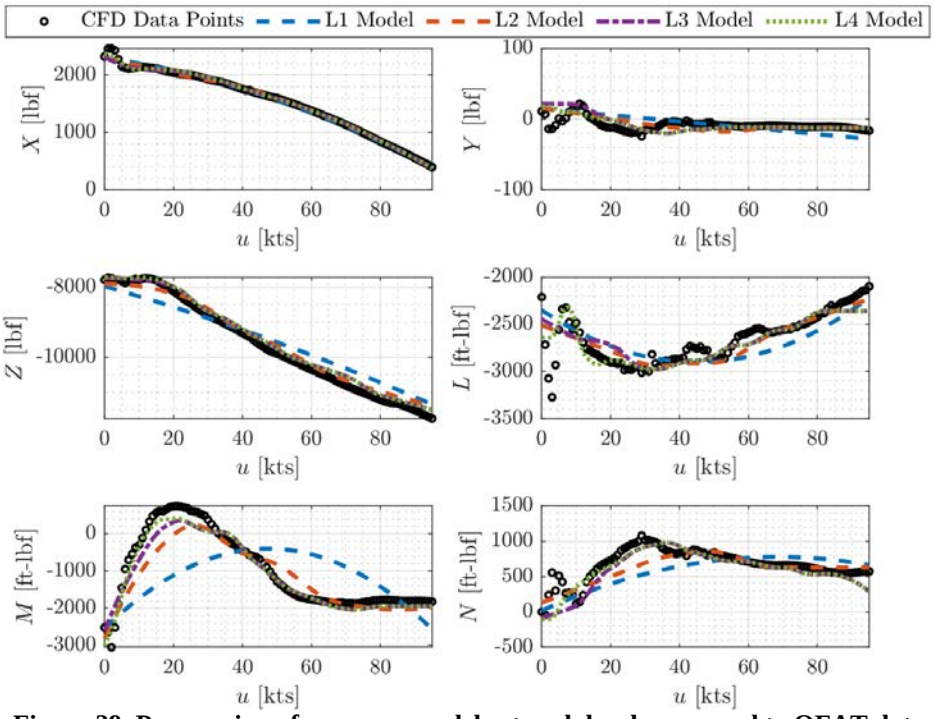

Figure 29. Progression of response models at each level compared to OFAT data.

Effectiveness of the modeling progression can also be seen in Fig. 29, where model responses are plotted against one-factor-at-a-time (OFAT) data. In this figure, all factors are fixed at their mid-range values in the model while the model responses can vary with body-axis velocity *u*. Plots for pitching moment, *M*, demonstrate the effective progression toward a good fit, where it can be observed that as model level increases, the response prediction significantly improves compared to the OFAT data. The roll moment, *L*, highlights some of the variability of the underlying data, particularly at very low speeds. SME judgement, in this case, would deem further splitting unnecessary and the models satisfactory. Figures 30a and 30b highlight examples of the longitudinal final blended global model response surfaces, as functions of (*u*, *v*) and (*u*, *w*), respectively, with color coding based on coefficient magnitude.

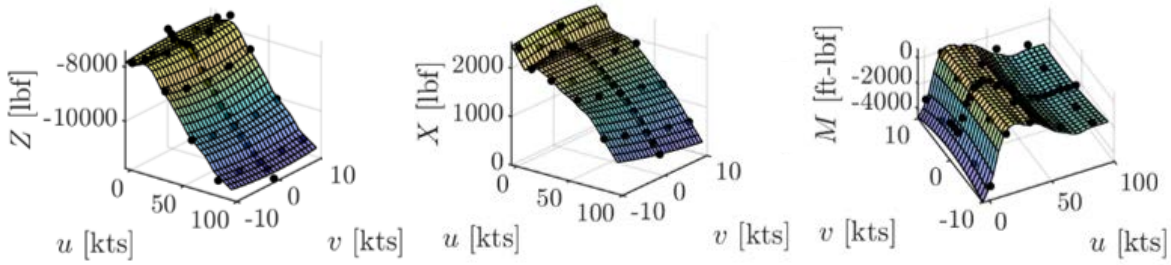

Figure 30a. Final global longitudinal response models as function of (*u, v*).

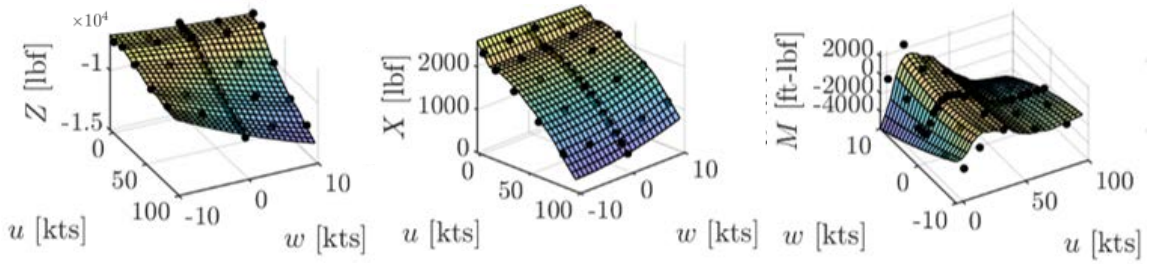

Figure 30b. Final global longitudinal response models as function of (*u, w*).

VI. Concluding Remarks

Aircraft complexity, both in numbers of factors and aerodynamic interactions, for hybrid aircraft-rotorcraft configurations, such as eVTOL, have motivated studies to develop an approach to testing and modeling that can guide the process in a more automated, efficient, and statistically rigorous fashion. Results toward that goal are presented in this paper by application of the RAM process to two different applications: a rotorcraft airfoil and a complex eVTOL design. Designed experiments based on DOE/RSM, contained in an automated RAM process demonstrate the method can provide statistical information before, during, and after the experiment is completed. The RAM-C process is particularly helpful to investigators working to obtain a specific desired level of model fidelity when working with high-fidelity computational codes. The sequential nature of the general RAM approach also inherently limits data collection to that required to match model complexity and fidelity requirements. In addition, for typical eVTOL vehicles where the number of factors may be 3-5 times that of a conventional aircraft, an automated RAM approach provides guidance starting with experiment design, through test execution, and in final model analysis. Examples of RAM-C have demonstrated an automated modeling process for static aerodynamic testing in a computational environment. Given the versatility of the RAM process to guide a wide spectrum of complex testing and modeling problems and the likely complex nature of vehicle designs in future UAM environments, this approach should be considered for future vehicle studies. Future work will further refine and extend the RAM process.

Acknowledgments

The authors extend their appreciation to the NASA Transformational Tools and Technologies, and Revolutionary Vertical Lift Technologies, Projects. Numerical simulations were performed using the NASA Advanced Supercomputing (NAS) System and the NASA Langley Research Center Mid-Range Computing Cluster.

References

[1] Booze Allen Hamilton, Final Report Urban Air Mobility (UAM) Market Study, https://ntrs.nasa.gov/archive/nasa/casi.ntrs.nasa.gov/ 20190001472.pdf .

[2] Crown Consulting, Inc., McKinsey & Company, Ascension Global, Georgia Tech, Urban Air Mobility (UAM) Market Study, https://www.nasa.gov/sites/default/files/atoms/files/uam-market-study-executive-summary-v2.pdf .

[3] Button, Keith, "For Vahana, A Study in Coping with Complexity," Aerospace America, June 2019.

[4] De Loach, R., "Applications of Modern Experiment Design to Wind Tunnel Testing at NASA Langley Research Center," AIAA 98-0713, *36th AIAA Aerospace Sciences Meeting and Exhibit*, Reno, NV, 1998.

[5] Morelli, E. A., and De Loach, R., "Ground Testing Results Using Modern Experiment Design and Multivariate Orthogonal Functions," AIAA 2003-0653, *41st AIAA Aerospace Sciences Meeting & Exhibit, Reno*, NV, 2003.

[6] Landman, Drew, Simpson, Jim, Vicroy, Dan, and Parker, Peter, "Response Surface Methods for Efficient Complex Aircraft Configuration Aerodynamic Characterization," *Journal of Aircraft*, Vol. 44, No. 4, July-August 2007. DOI: 10.2514/1.24810.

[7] Landman, Drew, Simpson, Jim, Mariani, Raffaello, Ortiz, Francisco, Britcher, Colin, "Hybrid Design for Aircraft Wind-Tunnel Testing Using Response Surface Methodologies," *Journal of Aircraft*, Vol. 44, No. 4, July-August 2007. DOI: 10.2514/1.25914.

[8] Landman, Drew, Simpson, Jim, Vicroy, Dan, and Parker, Peter, "Efficient Methods for Complex Aircraft Configuration Aerodynamic Characterization Using Response Surface Methodologies," *44th Aerospace Sciences Meeting and Exhibit*, January 2006. DOI: 10.2514/1.24810.

[9] Rothhaar, P., Murphy, P. C., Bacon, B. J., Grauer, J.; NASA Langley Distributed Propulsion VTOL Tilt Wing Aircraft Testing, Modeling, Simulation, Control, and Flight Test Development, AIAA AFM Conference, *AIAA Aviation 2014*, AIAA Paper No. 2014-2999.

[10] Busan, Ronald, Rothhaar, Paul, Croom, Mark, Murphy, Patrick C., Grafton, Sue, O'Neal, Anthony, "Enabling Advanced Wind-Tunnel Research Methods Using the NASA Langley 12-Foot Low Speed Tunnel," *AIAA Aviation and Aeronautics Forum and Exposition 2014*, AIAA Paper No. 2014-3000.
[11] Murphy, Patrick C. and Landman, Drew, "Experiment Design for Complex VTOL Aircraft with Distributed Propulsion and Tilt Wing," AIAA Atmospheric Flight Mechanics Conference, *AIAA SciTech 2015*, AIAA Paper No. 2015-0017.
[12] Murphy, Patrick C., Brandon, Jay, "Efficient Testing Combining Design of Experiment and Learn-to-Fly Strategies," AIAA SciTech Forum, *Atmospheric Flight Mechanics Conference*, AIAA 2017-0696, January 2017. DOI: 10.2514/6.2017-0696.
[13] Simpson, James R. and Wisnowski, James W., "Streamlining Flight Test with the Design and Analysis of Experiments," *Journal of Aircraft*, Vol. 38, No. 6, November-December 2001.
[14] Omran, Ashraf, Landman, Drew, Newman, Brett, "Global Stability and Control Derivative Modeling Using Design of Experiments," *AIAA Flight Mechanics Conference*, AIAA Paper No. 2009-5721, DOI: 10.2514/6.2009-5721.
[15] Brandon, Jay M., Morelli, Eugene A., "Nonlinear Aerodynamic Modeling From Flight Data Using Advanced Piloted Maneuvers and Fuzzy Logic," NASA/TM–2012-217778.
[16] Morelli, E. A., "Efficient Global Aerodynamic Modeling from Flight Data," *50th AIAA Aerospace Sciences Meeting*, AIAA Paper 2012-1050, January 2012.
[17] Brandon, J. M. and Morelli, E. A., "Real-Time Global Nonlinear Aerodynamic Modeling from Flight Data," *Journal of Aircraft*, Vol. 53, No. 5, September-October 2016, pp. 1261-1297.
[18] North, D. D., "Flight Testing of a Scale Urban Air Mobility Technology Testbed," *AIAA SciTech 2021 Forum*, Virtual Event, 2021. To be published.
[19] Williams, Brianne, Y., Landman, Drew, Flory, Isaac L., and Murphy, Patrick C., "The Effect of Systematic Error in Forced Oscillation Testing," *Aerospace Sciences Meeting*, AIAA Paper No. 2012-0768.
[20] Cummings, R.M. and Schütte, A., "Integrated Computational/Experimental Approach to Unmanned Combat Air Vehicle Stability and Control Estimation", *Journal of Aircraft*, Vol. 49, No. 6 (2012), pp. 1542-1557. doi: 10.2514/1.C03143.
[21] Ghoreyshi Mehdi, Cummings, Russell M., "Unsteady Aerodynamics Modeling for Aircraft Maneuvers: a New Approach Using Time-Dependent surrogate Modeling," *30th AIAA Applied Aerodynamics Conference*, AIAA 2012-3327, June, 2012.
[22] Murphy, P.C., Klein, V., Frink, Neal T., and Vicroy, Dan D., "System Identification Applied to Dynamic CFD Simulation and Wind-Tunnel Data," *AIAA Atmospheric Flight Mechanics Conference*, AIAA 2011-6522, August 2011.
[23] Murphy, Patrick C., Klein, Vladislav, Frink, Neal T.: Nonlinear Unsteady Aerodynamic Modeling Using Wind Tunnel and Computational Data. *Journal of Aircraft*. Vol. 54: 659-683, No. 2, March-April 2017. DOI: 10.2514/1.C033881.
[24] Frink, Neal T., Murphy, Patrick C., Atkins, Harold L., Viken, Sally A., Petrilli, Justin L.: Computational Aerodynamic Modeling Tools for Aircraft Loss-of-Control. *Journal of Guidance, Control, and Dynamics*. Vol. 40: 789-803, No. 4, April 2017. DOI: 10.2514/1 G001736.
[25] Derlaga, J. M., Jackson, C. W., and Buning, P. G., "Recent Progress in OVERFLOW Convergence Improvements," AIAA Paper 2020-1045, Jan. 2020.
[26] Buning, P. G., and Pulliam, T. H., "Near-Body Grid Adaption for Overset Grids," AIAA Paper 2016-3326, June 2016.
[27] P.G. Buning, R.J. Gomez, and W.I. Scallion, "CFD Approaches for Simulation of Wing-Body Stage Separation," AIAA-2004-4838, Aug. 2004.
[28] Geuther, S. C., and Fei, X., "LA-8 Computational Analysis and Validation Studies Using FlightStream," *AIAA SciTech 2021 Forum*, Virtual Event, 2021. To be published.
[29] North, D. D., Howland, G., and Busan, R. C. "Design and Fabrication of the LA-8 Distributed Electric Propulsion VTOL Testbed," *AIAA SciTech Forum*, January 2021 (to be published).
[30] Busan, R. C., Murphy, P. C., Hatke, D. B., and Simmons, B. M. "Wind Tunnel Testing Techniques for a Tandem Tilt-Wing, Distributed Electric Propulsion VTOL Aircraft," *AIAA SciTech Forum*, January 2021 (to be published).
[31] Simmons, B. M., and Murphy, P. C. "Wind Tunnel-Based Aerodynamic Model Identification for a Tilt-Wing, Distributed Electric Propulsion Aircraft," *AIAA SciTech 2021 Forum*, January 2021 (to be published).
[32] Simmons, B. M. "System Identification for Propellers at High Incidence Angles," *AIAA SciTech Forum*, January 2021 (to be published).
[33] Murphy, Patrick C., Hatke, David B., Aubuchon, Vanessa V., Weinstein, Rose, Busan, Ronald C., "Preliminary Steps in Developing Rapid Aero Modeling Technology," *AIAA Atmospheric Flight Mechanics Conference*, AIAA SciTech 2020, AIAA Paper No. 2020-0764.
[34] Murphy, P. C., Simmons, B. M., Hatke, D. B., Busan, R. C., "Rapid Aero Modeling for Urban Air Mobility Aircraft in Wind Tunnel Tests," *AIAA SciTech 2021 Forum*, January 2021 (to be published).
[35] Flemming, R. J., "An Experimental Evaluation of Advanced Rotorcraft Airfoils in the NASA Ames Eleven-Foot Transonic Wind Tunnel," NASA Contractor Report 166587, September 1984.
[36] Silva, C., Johnson, W. Antcliff, Kevin R., Patterson, Michael D., "VTOL Urban Air Mobility Concept Vehicles for Technology Development," 2018 Aviation Technology, Integration, and Operations Conference, *AIAA Aviation Forum*, June 25-29, 2018, Atlanta, Georgia.
[37] Fisher, Ronald A., "The Design of Experiments," 9th ed., Macmillan. ISBN 0-02-844690-9, 1971 (1935).
[38] Weinstein, R., and Hubbard, J. E., "Global Aerodynamic Modeling using Automated Local Model Networks in Real Time," AIAA Atmospheric Flight Mechanics Conference, *AIAA SciTech Forum*, January 2020, AIAA Paper 2020-0762.
[39] Montgomery, Douglas, C., "Design and Analysis of Experiments," 8th ed., Wiley, 2013.

[40] Box, G. E. P. and Wilson, K. B., "On the experimental attainment of optimum conditions," J. Roy. Statist. Soc., Ser. B Metho. Vol. 13, No. 1, pp. 1-45, 1951.
[41] Design Expert software, version 12, by Stat-Ease, www.statease.com.
[42] JMP software, version 14, by SAS Institute, www.jmp.com.
[43] Natoli, C., Burke, S., "Computer Experiments: Space Filling Design and Gaussian Process Modeling," STAT COE-Report-7-2018, Scientific Test and Analysis Techniques, Center of Excellence, www.afit.edu/STAT, Wright-Patterson AFB, OH.
[44] Klein, Vladislav and Morelli, Eugene A., "Aircraft System Identification: Theory and Practice," 1st edition, AIAA Inc., Reston, Virginia, 2006.
[45] De Loach, Richard, "Assessment of Response Surface Models Using Independent Confirmation Point Analysis," AIAA 2010-741, *48th AIAA Aerospace Sciences Meeting and Exhibit*, Orlando, FL, 2010.
[46] Ventura Diaz, P., and Yoon, S., "High-Fidelity Computational Aerodynamics of Multi-Rotor Unmanned Aerial Vehicles," AIAA Paper 2018-1266, Jan. 2018.
[47] Jia, Z., and Lee, S., "Acoustic Analysis of a Quadrotor eVTOL Design via High Fidelity Simulations," AIAA Paper 2019-2613, May 2019.
[48] Sandoz, Bryan, Vivek Ahuja, and Roy J. Hartfield. "Longitudinal Aerodynamic Characteristics of a V/STOL Tilt-wing Four-propeller Transport Model using a Surface Vorticity Flow Solver." *2018 AIAA Aerospace Sciences Meeting*. 2018. DOI:10.2514/6.2018-2070. http://openvsp.org/
[49] Johnson, Wayne R., "NDARC NASA Design and Analysis of Rotorcraft Validation and Demonstration," NASA/TP-2015-218751, https://ntrs.nasa.gov/search.jsp?R=20110002948 2020-05-28T21:05:53+00:00Z.
[50] Johnson, W. R. "CAMRAD II References," retrieved from http://johnson-aeronautics.com/documents/CAMRADreferences.pdf, Palo Alto, CA, 2018. https://software.nasa.gov/software/ARC-18184-1.
[51] Chaffin, M. S., & Berry, J. D., "Helicopter Fuselage Aerodynamics Under a Rotor by Navier-Stokes Simulation," Journal of the American Helicopter Society, Vol. 42, No. 3, pp. 235-243, 1997.